

Spectral distortions to the Cosmic Microwave Background from the recombination of hydrogen and helium

Wan Yan Wong^{1*}, Sara Seager^{2†} and Douglas Scott^{1‡}

¹*Department of Physics and Astronomy, University of British Columbia, 6224 Agricultural Rd., Vancouver, BC, V6T 1Z1, Canada*

²*Department of Terrestrial Magnetism, Carnegie Institution of Washington, 5241 Broad Branch Rd. NW, Washington, DC 20015, USA*

2005 October 19

ABSTRACT

The recombination of hydrogen and helium at $z \sim 1000$ – 7000 gives unavoidable distortions to the Cosmic Microwave Background (CMB) spectrum. We present a detailed calculation of the line intensities arising from the Ly α (2p–1s) and two-photon (2s–1s) transitions for the recombination of hydrogen, as well as the corresponding lines from helium. We give an approximate formula for the strength of the main recombination line distortion on the CMB in different cosmologies, this peak occurring at about $170 \mu\text{m}$. We also find a previously undescribed long wavelength peak (which we call the pre-recombination peak) from the lines of the 2p–1s transitions, which are formed before significant recombination of the corresponding atoms occurred. Detailed calculations of the two-photon emission line shapes are presented here for the first time. The frequencies of the photons emitted from the two-photon transition have a wide spectrum and this causes the location of the peak of the two-photon line of hydrogen to be located almost at the same wavelength as the main Ly α peak. The helium lines also give distortions at similar wavelengths, so that the combined distortion has a complex shape. The detection of this distortion would provide direct supporting evidence that the Universe was indeed once a plasma. Moreover, the distortions are a sensitive probe of physics during the time of recombination. Although the spectral distortion is overwhelmed by dust emission from the Galaxy, and is maximum at wavelengths roughly where the cosmic far-infrared background peaks, it may be able to tailor an experiment to detect its non-trivial shape.

Key words: lines: formation – cosmology: cosmic microwave background – cosmology: early universe – cosmology: theory – atomic processes – infrared: general.

1 INTRODUCTION

Physical processes in the plasma of the hot early Universe thermalize the radiation content, and this redshifts to become the observed Cosmic Microwave Background (CMB; see Scott & Smoot 2004, and references therein). Besides the photons from the radiation background, there were some extra photons produced from the transitions when the electrons cascaded down to the ground state after they recombined with the ionized atoms. The transition from a plasma to mainly neutral gas occurred because as the Universe expanded the background temperature dropped, allowing the ions to hold onto their electrons. The photons created in this process give a distortion to the nearly perfect blackbody CMB spectrum. Since recombination happens at redshift

$z \sim 1000$, then Ly α is observed at $\sim 100 \mu\text{m}$ today. There is approximately one of these photons per baryon, which should be compared with the $\sim 10^9$ photons per baryon in the entire CMB. However, the recombination photons are superimposed on the Wien part of the CMB spectrum, and so make a potentially measurable distortion.

From the Far-Infrared Absolute Spectrophotometer (FIRAS) measurements, Fixsen et al. (1996) and Mather et al. (1999) showed that the CMB is well modelled by a 2.725 ± 0.001 K blackbody, and that any deviations from this spectrum around the peak are less than 50 parts per million of the peak brightness. Constraints on smooth functions, such as μ - or y -distortions are similarly very stringent. However, there are much weaker constraints on narrower features in the CMB spectrum. Moreover, within the last decade it has been discovered Puget et al. (1996) that there is a Cosmic Infrared Background (CIB; see Hauser & Dwek 2001, and references therein), which peaks at 100 – $200 \mu\text{m}$ and is mainly composed of luminous infrared galaxies at moderate

* E-mail: wanyan@phas.ubc.ca

† E-mail: seager@dtm.ciw.edu

‡ E-mail: dscott@phas.ubc.ca

redshifts. The existence of this background makes it more challenging to measure the recombination distortions than would have been the case if one imagined them only as being distortions to Wien tail of the CMB. However, as we shall see, the shape of the recombination line distortion is expected to be much narrower than that of the CIB, and hence the signal may be detectable in a future experiment designed to measure the CIB spectrum in detail.

The first published calculations of the line distortions occur in the seminal papers on the cosmological recombination process by Peebles (1968) and Zel'dovich, Kurt & Sunyaev (1968). One of the main motivations for studying the recombination process was to answer the question: 'Where are the Ly α line photons from the recombination in the Universe?' (as reported in Rubino-Martin, Hernandez-Montegudo & Sunyaev 2005). In fact these studies found that for hydrogen recombination (in a cosmology which is somewhat different than the model favoured today) there are more photons created through the two-photon $2s-1s$ transition than from the Ly α transition. Both Peebles (1968) and Zel'dovich et al. (1968) plot the distortion of the CMB tail caused by these line photons, but give no detail about the line shapes. Other authors have included some calculation or discussion of the line distortions as part of other recombination related studies, e.g. Boschan & Biltzinger (1998), and most recently Switzer & Hirata (2005). However, the explicit line shapes have never before been presented, and the helium lines have also been neglected so far. The only numerical study to show the hydrogen lines in any detail is a short conference report by Dell'Antonio & Rybicki (1993), meant as a preliminary version of a more full study which never appeared. Although their calculation appears to have been substantially correct, unfortunately in the one plot they show of the distortions (their fig. 2) it is difficult to tell precisely which effects are real and which might be numerical.

Some of the recombination line distortions from higher energy levels, $n > 2$, have also been calculated (Dubrovich 1975; Lyubarsky & Sunyaev 1983; Fahr & Loch 1991; Burdzyuzha & Chekmezov 1994; Dell'Antonio & Rybicki 1993; Dubrovich & Stolyarov 1995, 1997; Burgin 2003; Kholupenko, Ivanchik & Varshalovich 2005). However, these high n lines are extremely weak compared with the CMB (below the 10^{-6} level), while the Ly α line is well above the CMB in the Wien region of the spectrum.

As trumpeted by many authors, we are now entering into the era of precision cosmology. Hence one might imagine that future delicate experiments may be able to measure these line distortions. Since the lines are formed by the photons emitted in each transitions of the electrons, they are strongly dependent on the rate of recombination of the atoms. The distortion lines may thus be a more sensitive probe of recombination era physics than the ionization fraction x_e , and the related visibility function which affects the CMB anisotropies. This is because a lot of energy must be injected in order for any physical process to change x_e substantially (e.g. Peebles, Seager & Hu 2000). In general that energy will go into spectral distortions, including boosting the recombination lines.

This also means that a detailed understanding of the physics of recombination is crucial for calculating the distortion. The basic physical picture for cosmological recom-

bination has not changed since the early work of Peebles (1968) and Zel'dovich et al. (1968). However, there have been several refinements introduced since then, motivated by the increased emphasis on obtaining an accurate recombination history as part of the calculation of CMB anisotropies. Seager, Sasselov & Scott (1999,2000) presented a detailed calculation of the whole recombination process, with no assumption of equilibrium among the energy levels. This multi-level computation involves 300 levels for both hydrogen and helium, and gives us the currently most accurate picture of the recombination history. In the context of the Seager et al. (2000) recombination calculation, and with the well-developed set of cosmological parameters provided by Wilkinson Microwave Anisotropy Probe (WMAP; Spergel et al. 2003) and other CMB experiments, it seems an appropriate time to calculate the distortion lines to higher accuracy in order to investigate whether they could be detected and whether their detection might be cosmologically useful.

The aim of this paper is to calculate the line distortions on the CMB from the $2p-1s$ and $2s-1s$ transitions of H and the corresponding lines of He (i.e. the 2^1p-1^1s and 2^1s-1^1s transitions of HeI, and the $2p-1s$ and $2s-1s$ transitions of HeII) during recombination, using the standard cosmological parameters and recombination history. In Section 2 we will describe the model we used in the numerical calculation and give the equations used to calculate the spectral lines. In Section 3 we will present our results and discuss the detailed physics of the locations and shapes of the spectral lines. An approximate formula for the magnitude of the distortion in different cosmologies will also be given. Other possible modifications of the spectral lines and their potential detectability will be discussed in Section 4. And finally, we will present our conclusions in the last section.

2 BASIC THEORY

2.1 Model

Instead of adopting a full multi-level code, we use a simple 3-level model atom here. For single-electron atoms (i.e. HI and HeII), we consider only the ground state, the first excited state and the continuum. For the 2-electron atom (HeI), we consider the corresponding levels among singlet states. In general, the upper level states are considered to be in thermal equilibrium with the first excited state. Case B recombination is adopted here, which means that we ignore recombinations and photo-ionizations directly to ground state. This is because the photons emitted from direct recombinations to the ground state will almost immediately reionize a nearby neutral H atom (Peebles 1968; Seager et al. 2000). We also include the two-photon rate from $2s$ to the ground state for all three atoms, with rates: $\Lambda_{2s-1s}^H = 8.229063 \text{ s}^{-1}$ (Goldman 1989; Santos, Parente & Indelicato 1998); $\Lambda_{2^1s-1^1s}^{\text{HeI}} = 51.02 \text{ s}^{-1}$ (Derevianko & Johnson 1997), although it makes no noticeable difference to the calculation if one uses the older value of 51.3 s^{-1} from Drake, Victor & Dalgarno (1969); and $\Lambda_{2s-1s}^{\text{HeII}} = 526.532 \text{ s}^{-1}$ (Lipeles, Novick & Tolk 1965; Goldman 1989). This 3-level atom model is similar to the one used in the program *recfast*, with the main difference being that here we do not assume that the rate of change of the first excited state n_2 is zero.

The rate equations for the 3 atoms are similar, and so we will just state the hydrogen case as an example:

$$(1+z)\frac{dn_1^{\text{H}}(z)}{dz} = -\frac{1}{H(z)}[\Delta R_{2\text{p}-1\text{s}}^{\text{H}} + \Delta R_{2\text{s}-1\text{s}}^{\text{H}}] + 3n_1^{\text{H}}; \quad (1)$$

$$(1+z)\frac{dn_2^{\text{H}}(z)}{dz} = -\frac{1}{H(z)}[n_e n_{\text{p}} \alpha_{\text{H}} - n_{2\text{s}}^{\text{H}} \beta_{\text{H}} - \Delta R_{2\text{p}-1\text{s}}^{\text{H}} - \Delta R_{2\text{s}-1\text{s}}^{\text{H}}] + 3n_2^{\text{H}}; \quad (2)$$

$$(1+z)\frac{dn_e(z)}{dz} = -\frac{1}{H(z)}[n_{2\text{s}}^{\text{H}} \beta_{\text{H}} - n_e n_{\text{p}} \alpha_{\text{H}}] + 3n_e; \quad (3)$$

$$(1+z)\frac{dn_{\text{p}}(z)}{dz} = -\frac{1}{H(z)}[n_{2\text{s}}^{\text{H}} \beta_{\text{H}} - n_e n_{\text{p}} \alpha_{\text{H}}] + 3n_{\text{p}}. \quad (4)$$

Here the values of n_i are the number density of the i th state, where n_e and n_{p} are the number density of electrons and protons respectively. $\Delta R_{i-j}^{\text{H}}$ is the net bound-bound rate between state i and j and the detailed form of $\Delta R_{2\text{p}-1\text{s}}^{\text{H}}$ and $\Delta R_{2\text{s}-1\text{s}}^{\text{H}}$ will be discussed in the next subsection. $H(z) \equiv \dot{a}/a$ is the Hubble factor,

$$H(z)^2 = H_0^2 \left[\frac{\Omega_{\text{M}}}{1+z_{\text{eq}}} (1+z)^4 + \Omega_{\text{M}} (1+z)^3 + \Omega_{\text{K}} (1+z)^2 + \Omega_{\Lambda} \right], \quad (5)$$

where Ω represents the fraction of the critical density in matter, curvature or cosmological constant, and the Hubble parameter today $H_0 = 100h \text{ km s}^{-1} \text{ Mpc}^{-1}$. Finally α_{H} is the Case B recombination coefficient from Hummer (1994),

$$\alpha_{\text{H}} = 10^{-19} \frac{at^b}{1+ct^d} \text{ m}^3 \text{ s}^{-1}, \quad (6)$$

which is fitted by Pequignot, Petitjean & (1991), with $a = 4.309$, $b = -0.6166$, $c = 0.6703$, $d = 0.5300$ and $t = T_{\text{M}}/10^4 \text{ K}$, while β_{H} is the photo-ionization coefficient:

$$\beta_{\text{H}} = \alpha_{\text{H}} \left(\frac{2\pi m_e k_{\text{B}} T_{\text{M}}}{h_{\text{p}}^2} \right)^{\frac{3}{2}} \exp \left\{ -\frac{h_{\text{p}} \nu_{2\text{s}-\text{c}}}{k_{\text{B}} T_{\text{M}}} \right\}, \quad (7)$$

where k_{B} is Boltzmann's constant, h_{p} is Planck's constant, m_e is the mass of electron, T_{M} is the matter temperature and $\nu_{2\text{s}-\text{c}}$ is the frequency of the energy difference between state 2s and the continuum. For the rate of change of T_{M} , we include only the Compton and adiabatic cooling terms (Seager et al. 2000), i.e.

$$(1+z)\frac{dT_{\text{M}}}{dz} = \frac{8\sigma_{\text{T}}U}{3H(z)m_e c} \frac{n_e}{n_e + n_{\text{H}} + n_{\text{He}}} (T_{\text{M}} - T_{\text{R}}) + 2T_{\text{M}}, \quad (8)$$

where T_{R} is the radiation temperature, c is the speed of light, $U = a_{\text{R}} T_{\text{R}}^4$, a_{R} is the radiation constant and σ_{T} is the Thompson scattering cross-section.

We use the Bader-Deuffhard semi-implicit numerical integration scheme (see Section 16.6 in Press et al. 1992) to solve the above rate equations. All the numerical results are made using the Λ CDM model with parameters: $\Omega_{\text{B}} = 0.046$; $\Omega_{\text{M}} = 0.3$; $\Omega_{\Lambda} = 0.7$; $\Omega_{\text{K}} = 0$; $Y_{\text{p}} = 0.24$; $T_0 = 2.725 \text{ K}$ and $h = 0.7$ (see e.g. Spergel et al. 2003). Here Y_{p} is the primordial He abundance and T_0 the present background temperature.

2.2 Spectral distortions

We want to calculate the specific line intensity $I_{\nu_0}(z=0)$ (i.e. energy per unit time per unit area per unit frequency per unit solid angle, measured in $\text{W m}^{-2} \text{ Hz}^{-1} \text{ sr}^{-1}$) observed at the present epoch, $z=0$. The detailed calculation of $I_{\nu_0}(z=0)$ for the Ly α transition and the two-photon transition in hydrogen are presented as examples (the notation follows Section 2.5 in Padmanabhan 1993). A similar derivation holds for the corresponding transitions in helium. To perform these calculations we first consider the emissivity $j_{\nu}(z)$ (energy per unit time per unit volume per unit frequency, measured in $\text{W m}^{-3} \text{ Hz}^{-1}$) of photons due to the transition of electrons between the 2p and 1s states at redshift z :

$$j_{\nu}(z) = h_{\text{p}} \nu \Delta R_{2\text{p}-1\text{s}}^{\text{H}}(z) \phi[\nu(z)], \quad (9)$$

where $\phi(\nu)$ is the frequency distribution of the emitted photons from the emission process and $\Delta R_{2\text{p}-1\text{s}}^{\text{H}}$ is the net rate of photon production between the 2p and 1s levels, i.e.

$$\Delta R_{2\text{p}-1\text{s}}^{\text{H}} = p_{12} (n_{2\text{p}}^{\text{H}} R_{21} - n_1^{\text{H}} R_{12}). \quad (10)$$

Here n_i^{H} is the number density of hydrogen atoms having electrons in state i , the upward and downward transition rates are

$$R_{12} = B_{12} \bar{J}, \quad (11)$$

$$\text{and } R_{21} = (A_{21} + B_{21} \bar{J}), \quad (12)$$

with A_{21} , B_{12} and B_{21} being the Einstein coefficients and p_{12} the Sobolev escape probability (see Seager et al. 2000), which accounts for the redshifting of the Ly α photons due to the expansion of the Universe. As $n_1^{\text{H}} \gg n_{2\text{p}}^{\text{H}}$, p_{12} can be expressed in the following form:

$$p_{12} = \frac{1 - e^{-\tau_{\text{s}}}}{\tau_{\text{s}}}, \text{ with} \quad (13)$$

$$\tau_{\text{s}} = \frac{A_{21} \lambda_{2\text{p}-1\text{s}}^3 (g_{2\text{p}}/g_1) n_1}{8\pi H(z)}. \quad (14)$$

We approximate the background radiation field \bar{J} as a perfect blackbody spectrum by ignoring the line profile of the emission (see Seager et al. 2000). We also neglect secondary distortions to the radiation field (but see the discussion in Section 4.1). These secondary distortions come from photons emitted earlier in time, during recombination of H or He, primarily the line transitions described in this paper. Assuming a blackbody we have

$$\bar{J}(T_{\text{M}}) = \frac{2h_{\text{p}} \nu_{\alpha}^3}{c^2} \left[\exp \left(\frac{h_{\text{p}} \nu_{\alpha}}{k_{\text{B}} T_{\text{M}}} \right) - 1 \right]^{-1}, \quad (15)$$

where $\nu_{\alpha} = c/121.5682 \text{ nm} = 2.466 \times 10^{15} \text{ Hz}$ and corresponds to the energy difference between states 2p and 1s, while the frequency of the emitted photons is equal to ν_{α} . Therefore, we can set $\phi[\nu(z)] = \delta[\nu(z) - \nu_{\alpha}]$, i.e. a delta function centred on ν_{α} , so that

$$j_{\nu}^{\text{Ly}\alpha}(z) = h_{\text{p}} \nu \Delta R_{2\text{p}-1\text{s}}^{\text{H}}(z) \delta[\nu(z) - \nu_{\alpha}]. \quad (16)$$

The increment to the intensity coming from time interval dt at redshift z is

$$dI_{\nu}(z) = \frac{c}{4\pi} j_{\nu} dt, \quad (17)$$

which redshifts to give

$$dI_{\nu_0}(z=0) = \frac{c}{4\pi} \frac{j_\nu}{(1+z)^3} dt.$$

We assume that the emitted photons propagate freely until the present time. Integration over frequency then gives

$$I_{\nu_0}^{\text{Ly}\alpha}(z=0) = \frac{c}{4\pi} \int \frac{j_\nu}{(1+z)^3} dt \quad (18)$$

$$= \frac{ch_p}{4\pi} \frac{\Delta R_{2p-1s}^{\text{H}}(z_\alpha)}{H(z_\alpha)(1+z_\alpha)^3}, \quad (19)$$

with

$$1+z_\alpha = \frac{\nu_\alpha}{\nu_0},$$

using

$$\nu(z) = \nu_0(1+z) \quad \text{and} \quad \frac{dt}{dz} = -\frac{1}{H(z)(1+z)}.$$

Equation (19) is the basic equation for determining the Ly α line distortion, using $\Delta R_{2p-1s}^{\text{H}}(z)$ from the 3-level atom calculation.

For the two-photon emission between the 2s and 1s levels, the emissivity at each redshift is

$$j_\nu(z) = h_p \nu \Delta R_{2s-1s}^{\text{H}}(z) \phi[\nu(z)], \quad (20)$$

and the calculation is slightly more complicated, since for $\phi(\nu)$ we need the frequency spectrum of the emission photons of the 2s–1s transition of H (Spitzer & Greenstein 1951; Martinis & Stojic 2000) as shown in Fig. 1. Here $\Delta R_{2s-1s}^{\text{H}}$ is the net rate of photon production for the 2s–1s transition, i.e.

$$\Delta R_{2s-1s}^{\text{H}} = \Lambda_{\text{H}} (n_{2s}^{\text{H}} - n_{1s}^{\text{H}} e^{-h_p \nu_\alpha / k_{\text{B}} T_{\text{M}}}). \quad (21)$$

Therefore, using equation (18), we have

$$I_{\nu_0}^{2\gamma}(z=0) = \frac{ch_p \nu_0}{4\pi} \int_0^\infty \frac{\Delta R_{2s-1s}^{\text{H}}(z) \phi[\nu_0(1+z)]}{H(z)(1+z)^3} dz. \quad (22)$$

We use the simple trapezoidal rule (see Section 4.1 in Press et al. 1992) to integrate equation (22) numerically from $z=0$ to the time when ΔR is sufficiently small that the integrand can be neglected.

3 RESULTS

Each of the line distortions are shown separately in Fig. 2 and summed for each species in Fig. 3. The shape of the lines from H, HeI and HeII are fairly similar. There are two distinct peaks to the 2p–1s emission lines. We refer to the one located at longer wavelength as the ‘pre-recombination peak’, since the corresponding atoms had hardly started to recombine during that time. The physics of the formation of this peak will be discussed in detail in section 3.1.1. The second (shorter wavelength) peak is the main recombination peak, which was formed when the atoms recombined. While the longer wavelength peak actually contains almost an order of magnitude more flux, it makes a much lower relative distortion to the CMB. The ratio of the total distortion to the CMB intensity is shown in Fig. 4. It is approximately one for the main recombination peak, but $\sim 10^{-4}$ for the pre-recombination peak.

In Fig. 3, we plot the lines from H and HeI together with

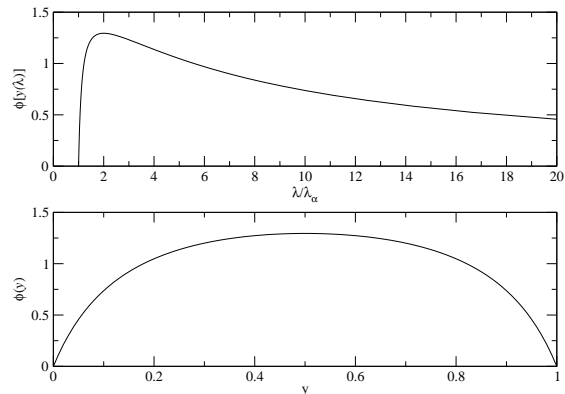


Figure 1. The normalized emission spectrum for the two-photon process (2s–1s) of hydrogen (Spitzer & Greenstein 1951; Martinis & Stojic 2000). The top panel shows $\phi[y(\lambda)]$ vs λ , while the bottom panel shows $\phi(y)$ vs y , where $\nu = y\nu_\alpha$. Note that the spectrum is symmetric in ν about $\nu_\alpha/2$, but the λ spectrum is very asymmetric, being zero below λ_α , and having a tail extending to high λ .

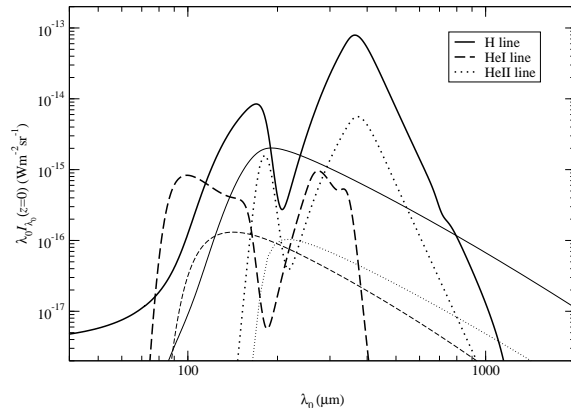


Figure 2. The line intensity $\lambda_0 I_{\lambda_0}$ from the net Ly α emission of H (thick solid), the two-photon emission (2s–1s) of H with the spectrum $\phi(\nu)$ (thin solid), the $2^1\text{p}-1^1\text{s}$ emission of HeI (thick dashed), the $2^1\text{s}-1^1\text{s}$ two-photon emission of HeI (thin dashed), the $2\text{p}-1\text{s}$ emission of HeII (thick dotted) and the $2\text{s}-1\text{s}$ two-photon emission of HeII (thin dotted).

the CMB and an estimate of the CIB. We can see that the lines which make the most significant distortion to the CMB are the Ly α line and the $2^1\text{p}-1^1\text{s}$ line of HeI, and that these lines form a non-trivial shape for the overall distortion. The sum of all the spectral lines and the CMB is shown in Fig. 3. Note that these lines will also exist in the presence of the CIB – but the shape of this background is currently quite poorly determined (Fixsen et al. 1998; Hauser et al. 1998).

We now discuss details of the physics behind the shapes of each of the main recombination lines.

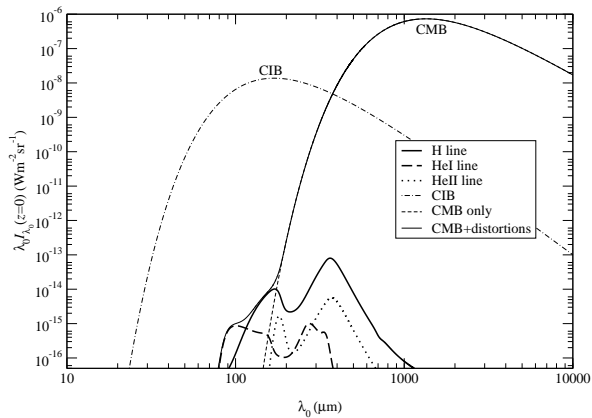


Figure 3. The line intensity $\lambda_0 I_{\lambda_0}$ from the sum of the net Ly α emission and two-photon emission (1s–2s) of H (thick solid), the sum of the 2^1p-1^1s emission and 2^1s-1^1s two-photon emission of HeI (thick dashed), and the sum of the 2p–1s emission and 2s–1s two-photon emission of HeII (thick dotted), together with the background spectra: CMB (long-dashed); and estimated CIB (dot-dashed; Fixsen et al. 1998). The sum of all the above emission lines of H and He plus the CMB is also shown (thin solid).

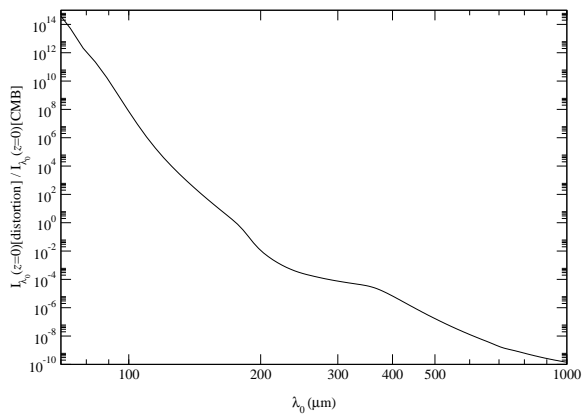


Figure 4. The ratio of the total line distortion to the CMB intensity is plotted. The ratio is larger than 1 (i.e. the intensity of the distortion line is larger than that of the CMB) when $\lambda_0 \sim 170 \mu\text{m}$ which is just where the main Ly α line peaks.

3.1 Lines from the recombination of hydrogen

During recombination, the Lyman lines are optically thick, which means that photons emitted from the transition to $n = 1$ are instantly reabsorbed. However, some of the emitted photons redshift out of the line due to the expansion of the Universe and this makes the Ly α transition one of the possible ways for electrons to cascade down to the ground state. The other path for electrons going from $n = 2$ to $n = 1$ is the two-photon transition between 2s and 1s. Fig. 5 shows the net photon emission rate of the Ly α and two-photon transitions as a function of redshift for the standard Λ CDM model. The two-photon rate dominates at low redshift, where the bulk of the recombinations occur. This means that there are more photons emitted through the two-photon emission process (54% of the total number of

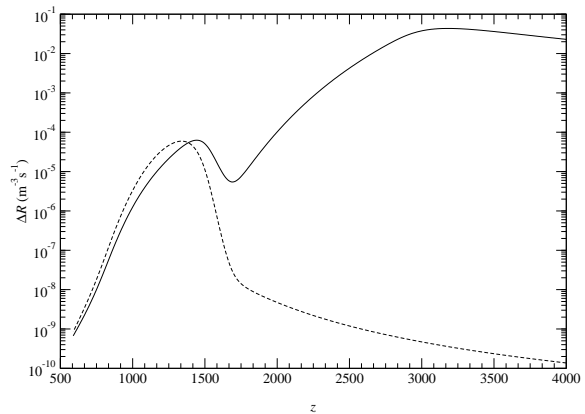


Figure 5. Comparison of the net 2p–1s (solid) and 2s–1s (dashed) transition rates of H. The Ly α redshifting process dominates during the start of recombination, while the 2-photon process is higher during most of the time that recombination is occurring. It turns out that in the standard Λ CDM model about equal numbers of hydrogen atoms recombine through each process, with slightly over half the hydrogen in the Universe recombining through the 2-photon process.

photons created during recombination of H) than through the Ly α redshifting process. This conclusion agrees with Zel’dovich et al. (1968) – although of course the balance depends on the cosmological parameters (see Seager et al. 2000) and for today’s best fit cosmology the two processes are almost equal. Despite this fact, the overall strength of the two-photon emission lines are weaker because the photons are not produced with a single frequency, but with a wide spectrum ranging from 0 to ν_α . The location of the two-photon peak (see Fig. 2) is also somewhat unexpected, since it is almost at the same wavelength as the Ly α recombination peak, rather than at twice the wavelength. The reason for this will be discussed in section 3.1.2.

We should also note that the tiny dip in our curves for the long-wavelength tail of the pre-recombination peak (see Fig. 2) is due to a numerical error, when the number density of the ground state is very small. This can also be seen in the pre-recombination peak for HeII.

3.1.1 The pre-recombination emission peak

The highest Ly α peak (shown in Fig. 2) is formed before the recombination of H has already started, approximately at $z > 2000$. During that time the emission of Ly α photons is controlled by the bound-bound Ly α rate from $n = 2$ (i.e. the $n_2 R_{21}$ term in equation (10)) and the photo-ionization rate ($n_2 \alpha_H$). From Fig. 6, we can see that at early times the bound-bound Ly α rate is larger than the photo-ionization rate. This indicates that when an electron recombines to the $n = 2$ state, it is more likely to go down to the ground state by emission of a Ly α photon than to get ionized. The excess Ly alpha photons are not reabsorbed by ground state H, but are redshifted out of the absorption frequency due to the expansion of the Universe; they escape freely and form the pre-recombination emission line. Note that there is very little net recombination of H, since the huge reservoir

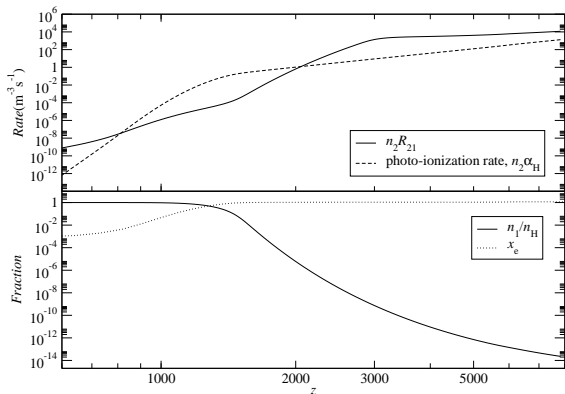


Figure 6. The top panel shows the bound-bound Ly α rate $n_2 R_{21}$ and the photo-ionizing rate $n_2 \alpha_{\text{H}}$ for $n=2$. The lower panel shows the fraction of ground state H atoms n_1/n_{H} , and also the ionization fraction x_e .

of > 13.6 eV CMB photons keeps photo-ionizing the ground state H atoms (see Fig. 12).

We now turn to a more detailed explanation of the pre-recombination emission peak. The bound-bound Ly α rate from $n = 2$ is initially approximately constant, as it is dominated by the spontaneous de-excitation rate (the A_{21} term in equation (21)). At the same time the photo-ionization rate is always decreasing as redshift decreases, since the number of high energy photons keeps decreasing with the expansion of the Universe. Therefore, with a constant bound-bound Ly α rate and the decreasing photo-ionization rate, the emission of Ly α photons rises. The peak of this pre-recombination line of H occurs at around $z = 3000$, by which time only a very tiny amount of ground state H atoms have formed ($n_1/n_{\text{H}} < 10^{-7}$, see Fig. 6). These ground state H atoms build up until they can reabsorb the Ly α photons and this lowers the bound-bound Ly α rate. The decrease of the bound-bound Ly α rate is represented in the Sobolev escape probability p_{12} in equation (13). At high redshift, p_{12} is 1 and there is no trapping of Ly α photons. When H starts to recombine, the optical depth τ_s increases and the Ly α photons can be reabsorbed by even very small amounts of neutral H. For $\tau_s \gg 1$, we can approximate $p_{12} \simeq 1/\tau_s$ and $p_{12} \propto H(z)/n_1$. Because of the increase in the number density of the ground state and the decrease in $H(z)$, the pre-recombination line decreases. One can therefore think of the ‘pre-recombination peak’ as arising from direct Ly α transitions, before enough neutral H has built up to make the Universe optically thick for Lyman photons. This process occurs because the spontaneous emission rate (A_{21} term) is faster than the photoionization rate for $n = 2$; it increases as the Universe expands, due to the weakening CMB blackbody radiation, and is quenched as the fraction of atoms in the $n = 1$ level grows. The shorter wavelength peak, on the other hand, comes from the process of redshifting out of the Ly α line during the bulk of the recombination epoch.

By using the RECFAST program (Seager et al. 1999), we can generate the main Ly α recombination peak and also the two-photon emission spectrum, by simply adding a few lines into the code. However, the pre-recombination peak

cannot be generated from RECFAST, since there the rate of change of the number density of the first excited state n_2 is assumed to be negligible and is related to n_1 via thermal equilibrium. Moreover, in the effective 3-level formalism, the Ly α line is assumed to be optically thick throughout the whole recombination process of H (in order to reduce the calculation into a single ODE), which is not valid at the beginning of the recombination process. Hence, one needs to follow the rate equations of both states (i.e. $n = 1$ and $n = 2$) to generate the full Ly α emission spectrum. The pre-recombination peak of H was mentioned and plotted in the earlier work of Dell’Antonio & Rybicki (1993) as well, although they did not describe it in any detail.

Another way to understand the line formation mechanism is to ask how many photons are made in each process *per atom*. We find that for the main Ly α peak there are approximately 0.47 photons per hydrogen atom (in the standard cosmology). During the recombination epoch, net photons for the $n = 2$ to $n = 1$ transitions are only made when atoms terminate at the ground state. Hence we expect exactly one $n = 2$ to $n = 1$ photon for each atom, split between the Ly α redshifting and 2-photon processes (and the latter splits the energy into two photons, so there are 1.06 of these photons per atom). For the ‘pre-recombination peak’, on the other hand, the atoms give a Ly α photon when they reach $n = 1$, but they then absorb a CMB continuum photon to get back to higher n or become ionized. The number of times an atom cycles through this process depends on the ratio of the relevant rates. If we take the rate per unit volume from Fig. 5 and divide by the number density of hydrogen atoms at $z \simeq 3000$ then we get a rate which is about an order of magnitude larger than the Hubble parameter at that time. Hence we expect about 10 ‘pre-recombination peak’ photons per hydrogen atom. A numerical calculation gives the more precise value of 8.11.

3.1.2 The two-photon emission lines

Surprisingly, the location of the peak of the line intensity of the 2s–1s transition is almost the same as that of the Ly α transition, as shown in Fig. 2, while one might have expected it to differ by a factor of 2. In order to understand this effect, we rewrite the equation (22) in the following way:

$$I_{\nu_0}^{2\gamma}(z=0) = \int_0^\infty \phi'(z') I_{\nu_0}^\delta(z=0; z') dz', \quad (23)$$

where $\phi(z') = \nu_0 \phi(\nu')$, and

$$I_{\nu_0}^\delta(z=0; z') \equiv I_{\nu_0}^\delta(z=0; z'(\nu')) = \frac{ch_p}{4\pi} \frac{R_{2\gamma}(z')}{H(z')(1+z')^3}, \quad (24)$$

with

$$1+z' = \frac{\nu'}{\nu_0}.$$

Equation (24) gives the redshifted flux (measured now at $z = 0$) of a single frequency ν' coming from redshift z' and corresponding to the redshifted frequency ν_0 .

We first calculate the line intensity of the two-photon emission with a simple approximation: a delta function spectrum $\delta(\nu - \nu_\alpha/2)$, where $\nu_\alpha/2$ is the frequency corresponding to the peak of the two-photon emission spectrum $\phi(\nu)$. Fig. 7 shows the intensity spectrum of two-photon emission using

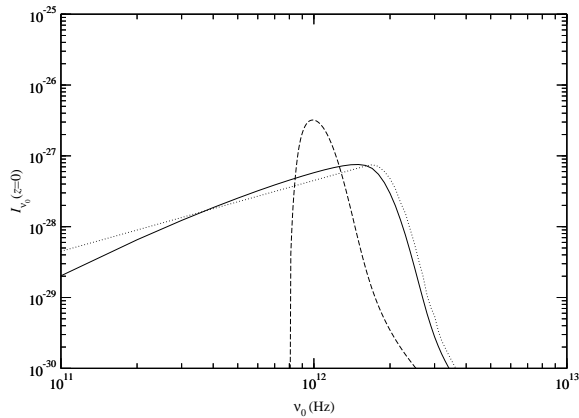


Figure 7. The line intensity of the 2s–1s transition (two-photon emission) $I_{\nu_0}(z=0)$ as a function of redshifted frequency ν_0 for three different assumptions: the correct frequency spectrum of two-photon emission (solid); the delta function approximation $\delta(\nu - \nu_\alpha/2)$ (dashed); and the flat spectrum approximation (dotted).

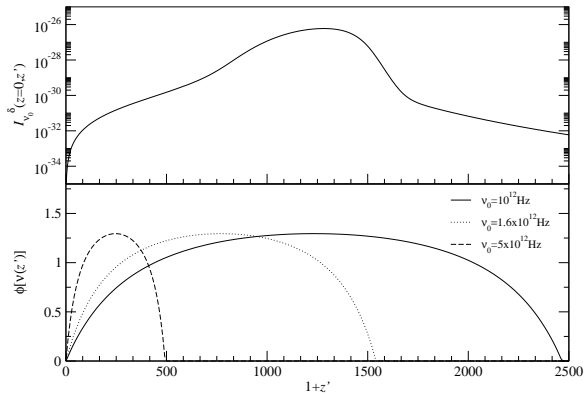


Figure 8. The top panel shows the redshifted flux from single emission frequency $I_{\nu_0}^{\delta}(z=0; z')$ plotted against the redshift of emission, $1+z'$. The bottom panel shows the frequency spectrum of two-photon emission $\phi[\nu(z')]$ plotted against z' for three redshifted frequencies: $\nu_0 = 10^{12}$ Hz; 1.6×10^{12} Hz; and 5×10^{12} Hz.

a delta frequency spectrum $\delta(\nu - \nu_\alpha/2)$ compared with the two-photon emission using the correct spectrum $\phi(\nu)$. We can see that there is a significant shift in the line centre compared with the δ -function case. Where does this shift come from?

We know that the frequencies of emitted photons are within the range of 0 to ν_α at the time of emission. For a fixed redshifted frequency ν_0 now, we can calculate the range of emission redshifts contributing to ν_0 (referred to as the ‘contribution period’ from now on), which is represented by $\phi'(z')$ or $\phi(\nu')$. In Fig. 8, we show the spectral distribution $\phi[\nu'(z')]$ as a function of redshift z' for specific values of ν_0 . For example, if we take $\nu_0 = 5 \times 10^{12}$ Hz, then photons emitted between $1+z = 1$ (i.e. $\nu = \nu_0$) and ~ 500 ($\nu = \nu_\alpha$) will give contributions to ν_0 . The smaller the redshifted frequency ν_0 , the wider the contribution period.

We might expect that the line intensity of this two-photon emission will be larger if the contribution period is longer, as there are more redshifted photons propagating from earlier times. However, this is not the case, because the rate of two-photon emission $R_{2\gamma}$ also varies with time, and is sharply peaked at $z \simeq 1300$ – 1400 . Hence $I_{\nu_0}^{\delta}(z=0; z')$ is also sharply peaked at $z \simeq 1300$ – 1400 . In Fig. 8, the redshifted flux integrand $I_{\nu_0}^{\delta}(z=0, z)$ and the emission spectrum $\phi[\nu(z)]$ are plotted on the same redshift scale. For $\nu_0 = 5 \times 10^{12}$ Hz (lowest panel), we can see that the contribution period covers a redshift range when $I_{\nu_0}^{\delta}(z=0, z)$ and $R_{2\gamma}$ are small in value. The contribution period widens with decreasing ν_0 and covers more of the redshift range when two-photon emission is high. Therefore, the flux $I_{\nu_0}(z=0)$ is expected to increase with decreasing ν_0 until the contribution period extends to the redshifts at which the two-photon emission peaks. As ν_0 gets even smaller (e.g. $\nu_0 = 10^{12}$ Hz), then the contribution period becomes larger than the redshift range for two-photon emission and hence only lower energy photons can be redshifted to that redshifted frequency. As a result, the flux $I_{\nu_0}(z=0)$ starts to decrease, and so we have a peak. The flux peaks at $\nu_0 \simeq 10^{12}$ Hz when we use the δ -function approximation. However, from Fig. 8, we can see that the contribution period for $\nu_0 \simeq 10^{12}$ Hz is much greater than that of the two-photon emission period, and therefore this is not the location of peak. Based on the argument presented above, we expect the peak to be at around 1.6×10^{12} Hz, or $200 \mu\text{m}$.

The basic mathematical point is that $\phi(y)$ is extremely poorly represented by a δ -function. Since the spectrum $\phi(\nu)$ is quite broad, it can be better approximated as a uniform distribution than as a δ -function. Another crude approximation would be to assume a flat spectrum for $\phi(\nu)$ in Fig. 1. Fig. 7 compares the intensity $I_{\nu_0}(z=0)$ found using the correct form for $\phi(\nu)$ with the δ -function and flat spectrum approximations. This shows that the flat spectrum gives qualitatively the same results as the correct form of the spectrum, and that the peak occurs fairly close to that of Ly α , but is much broader. The same general arguments apply to the two-photon lines of HeI and HeII (as we discuss in Section 3.2).

3.1.3 Dependence of Ω_M and Ω_B

The largest distortion on the CMB is from the shorter wavelength recombination peak of the hydrogen Ly α line (see Fig. 4). It may therefore be useful to estimate the peak of this line’s intensity as a function of the cosmological parameters. The relevant parameters are the matter density ($\propto \Omega_M h^2$) and the baryon density ($\propto \Omega_B h^2$). This is because $\Omega_M h^2$ affects the expansion rate, while $\Omega_B h^2$ is related to the number density of hydrogen. No other combinations of cosmological parameters have a significant impact on the physics of recombination.

We can crudely understand the scalings of these parameters through the following argument. Regardless of the escape probability p_{12} , the remaining part of the rate ($n_{2p}^H R_{21} - n_1^H R_{12}$) is roughly proportional to $n_1^H \propto \Omega_B h^2 (1 - x_e)$. The escape probability p_{12} can be approximated as 1 at the beginning of recombination ($\tau_s \ll 1$) and $1/\tau_s$ during the bulk of the recombination process (with $\tau_s \gg 1$). Note that $\tau_s \propto H(z)/n_1^H \propto (\Omega_M h^2)^{1/2} [\Omega_B h^2 (1 - x_e)]^{-1}$. Therefore,

$$\Delta R_{2p-1s} \propto \begin{cases} (\Omega_M h^2)^0 [\Omega_B h^2 (1 - x_e)] & \text{for } \tau_s \ll 1 \\ (\Omega_M h^2)^{1/2} [\Omega_B h^2 (1 - x_e)]^0 & \text{for } \tau_s \gg 1, \end{cases} \quad (25)$$

and thus

$$I_{\lambda_0} \propto \frac{\Delta R}{H(z)} \propto \begin{cases} (\Omega_M h^2)^{-1/2} [\Omega_B h^2 (1 - x_e)] & \text{for } \tau_s \ll 1 \\ (\Omega_M h^2)^0 [\Omega_B h^2 (1 - x_e)]^0 & \text{for } \tau_s \gg 1. \end{cases} \quad (26)$$

From this rough scaling argument, we may expect that the Ω_M dependence of the peak of the Ly α line is an approximate power law with index between $-1/2$ and 0 , while for Ω_B the corresponding power-law index is expected to lie between 0 and 1 . The dependence of Ω_M is actually more complicated when one allows for a wider range of values (see Dell’Antonio & Rybicki 1993). The above estimation just gives a rough physical idea of the power of the dependence.

A more complete numerical estimate of the peak of the recombination Ly α distortion is:

$$(\lambda_0 I_{\lambda_0})^{\text{peak}} \simeq 8.5 \times 10^{-15} \left(\frac{\Omega_B h^2}{0.0224} \right)^{0.57} \left(\frac{\Omega_M h^2}{0.147} \right)^{0.15} \text{ Wm}^{-2} \text{sr}^{-1}, \quad (27)$$

where we have normalized to the parameters of the currently favoured cosmological model. The peak occurs at

$$\lambda_0 \simeq 170 \mu\text{m} \quad (28)$$

for all reasonable variants of the standard cosmology.

3.2 Lines from the recombination of helium (HeI and HeII)

We compute the recombination of HeII and HeI in the same way as for hydrogen. For the two-electron atom HeI, we ignore all the forbidden transitions between singlet and triplet states due to the low population of the triplet states (see Seager et al. 1999, 2000). The 2^1p-1^1s transitions of HeI are optically thick, the same situation as for H. This makes the electrons take longer to reach the ground state and causes the recombination of HeI to be slower than Saha equilibrium. However, unlike for H, and despite the optically thick 2^1p-1^1s transition line, the 2^1p-1^1s rate dominates, as shown in Fig. 9. For HeII, due to the fast two-photon transition rate (see Fig. 10), there is no ‘bottleneck’ at the $n = 2$ level in the recombination process. Hence HeII recombination can be well approximated by using the Saha equilibrium formula (Seager et al. 2000).

We can see the effect of the above differences in recombination history on the lines: the width of the recombination peak of both H and HeI is larger than that of HeII. Overall, the spectral lines of HeI are of much lower amplitude than those of H (see Fig. 2) with the distortion to the CMB about an order of magnitude smaller.

The peaks of the line distortions from H and HeII are located at nearly the same wavelengths. For hydrogenic ions the $1s-2p$ energy (and all the others) scales as Z^2 , where Z is the atomic number. Hence for HeII recombination takes place at $z \simeq 6000$ rather than the $z \simeq 1500$ for hydrogen. Hence the line distortion from the $2p-1s$ transition of HeII redshifts down to about $200 \mu\text{m}$, just like Ly α .

The two-photon frequency spectrum of HeII is the same as for H, since they both are single-electron

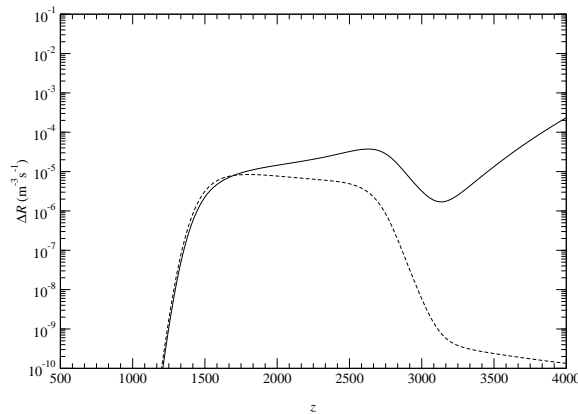


Figure 9. Comparison of the net 2^1p-1^1s (solid) and 2^1s-1^1s two-photon (dashed) transition rates of HeI. The two-photon rate is sub-dominant through most of the HeI recombination epoch, and hence, unlike for hydrogen, most helium atoms did *not* recombine through the two-photon process.

atoms (Tung et al. 1984). However, it is complicated to calculate the two-photon frequency spectrum of HeI very accurately, since there is no exact wave-function for the state of the atom. Drake et al. (1969) used a variational method to calculate the two-photon frequency spectrum of HeI with values given up to 3 significant figures. Drake (1986) presented another calculation, giving one more digit of precision, and making the spectrum smoother, as shown in Fig. 11. These two calculations differ by only about 1%, which makes negligible change to the two-photon HeI spectral line.

All of the H and He lines (for $n = 2$ to $n = 1$) are presented in Fig. 2 and the sum is shown as a fractional distortion to the CMB spectrum in Fig. 4. We find that in the standard cosmological model, for HeI recombination, there are about 0.67 photons created per helium atom in the ‘main’ 2^1p-1^1s peak, 0.70 per helium atom in the ‘pre-recombination peak’, and 0.66 in the two-photon process. The numbers for HeII recombination are 0.62, 0.76 and 6.85 for these three processes, respectively.

4 DISCUSSION

4.1 Modifications in the recombination calculation

There are several possible improvements that we could make to the line distortion calculation. However, as we will discuss below, we do not believe that any of them will make a substantial difference to the amplitudes of the lines.

In order to calculate the distortion lines to higher accuracy, we should use the multi-level model without any thermal equilibrium assumption among the bound states. And we also need to take into account the secondary spectral distortion in the radiation field, i.e. we cannot approximate the background radiation field \bar{J} as a perfect blackbody spectrum. This means, for example, that the extra photons from the recombination of HeI may redshift into an energy range that can photoionize H($n = 1$) (Dell’Antonio & Rybicki 1993; Seager et al. 2000). We can assess how significant

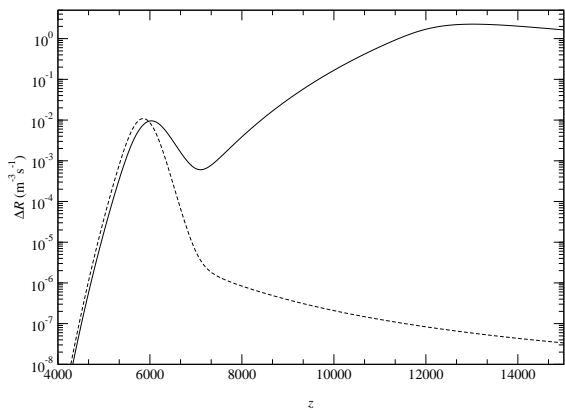


Figure 10. Comparison of the net 2p–1s (solid) and 2s–1s two-photon (dashed) transition rates of HeII as a function of redshift. The two-photon process is greater through most of the recombination epoch, so that most of the cosmological HeIII \rightarrow HeII process happens through the two-photon transition.

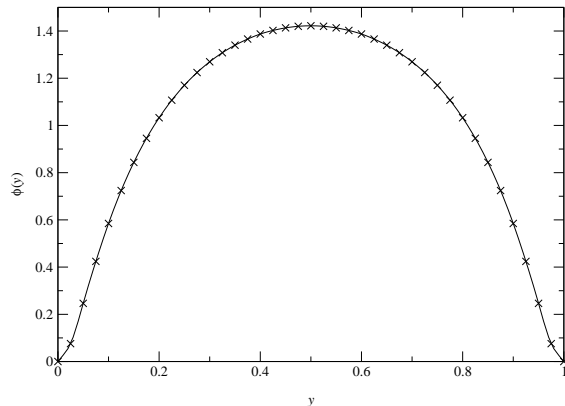


Figure 11. The normalized emission spectrum for the two-photon emission process (2^1s-1^1s) in HeI. Here $y = \nu/\nu_{2s-1s}$, where $\nu_{2s-1s} = 4.9849 \times 10^{15}$ Hz. The crosses are the calculated points from Drake et al. (1969) and Drake (1986), while the line is a cubic spline fit.

this effect might be by considering the ratio of the number of CMB background photons with energy larger than E_γ , $n_\gamma(> E_\gamma)$, to the number of baryons, n_B , at different redshifts (see Fig. 12).

Roughly speaking, the recombination of H occurs at the redshift when $n_\gamma(> h_p\nu_\alpha)/n_B$ is about equal to 1. This is because at lower redshifts there are not enough high energy background photons to photo-ionize or excite electrons from the ground state to the upper states (even to $n = 2$), while at higher redshift, when such transitions are possible, there are huge numbers of photons able to ionize the $n = 2$ level. The solid line in Fig. 12 shows the effect of the helium line distortions on the number of high energy photons (above Ly α) per baryon. The amount of extra distortion photons with redshifted energy larger than $h_p\nu_\alpha$ coming from the recombination of HeI is only about 1 per cent of the number of hydrogen atoms. Their effect is therefore expected to be

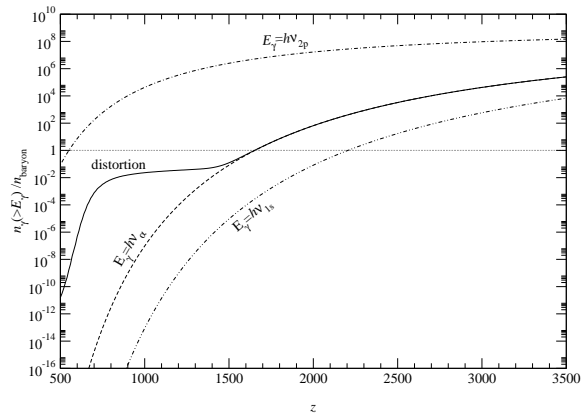


Figure 12. The ratio of number of CMB photons with energy larger than E_γ ($n_\gamma(> E_\gamma)$) to number of baryons (n_B) is plotted against redshift z . The solid line includes the extra distortion photons from the recombination of HeI. From the graph, we can see that the recombination of H occurs approximately at the redshift when the ratio of photons with energy $> h\nu_\alpha$ to baryons is about unity. By the time the helium recombination photons are a significant distortion to the CMB tail above Ly α the density of the relevant photons has already fallen by 2 orders of magnitude, and so the effects can make only a small correction.

negligibly small for x_e . We neglect the effect of the helium recombination photons on the hydrogen line distortion, since it is clearly going to make a small correction (at much less than the 10 per cent level).

As well as this particular approximation, there have been some other recent studies which have suggested that it may be necessary to make minor modifications to the recombination calculations presented in Seager et al. (1999, 2000). Although these proposed modifications would give only small changes to the recombination calculation, it is possible that they could have much more significant effects on the line amplitudes and shapes. Recent papers have described 3 separate potential effects.

In the effective three-level model, Leung, Chan & Chu (2004) argued that the adiabatic index of the matter should change during the recombination process, as the ionized gas becomes neutral, giving slight differences in the recombination history. Dubrovich & Grachev (2005) have claimed that the two-photon rate between the lowest triplet state and the ground state and that between the upper singlet states and the ground state should not be ignored in the recombination of HeI. And Chluba & Sunyaev (2005) suggested that one should also include stimulated emission from the 2s state of H, due to the low frequency photons in the CMB blackbody spectrum. Even if all of these effects are entirely completely correct, we find that the change to the amplitude of the main spectral distortion is much less than 10 per cent. We therefore leave the detailed discussion of these and other possible modifications to a future paper.

4.2 Possibility of detection

There is no avoiding the fact that detecting these CMB spectral distortions will be difficult. There are 3 main challenges to overcome: (1) achieving the required raw sensitivity; (2)

removing the Galactic foreground emission; and (3) distinguishing the signal from the CIB.

Let us start with the first point. We can estimate the raw sensitivity achievable in existing or planned experiments (even although these instruments have *not* been designed for measuring the line distortion). Since the relevant wavelength range is essentially impossible to observe from the ground, it will be necessary to go into space, or at least to a balloon-based mission. One existing experiment with sensitivity at relevant wavelengths is BLAST (Devlin et al. 2004), which has an array of bolometers operating at $250\ \mu\text{m}$ on a balloon payload. The estimated sensitivity is $236\ \text{mJy}$ in $1\ \text{s}$, for a $30\ \text{arcsec}$ FWHM beam, which corresponds to $\lambda I_\lambda = 1.2 \times 10^{-7}\ \text{W m}^{-2}\text{sr}^{-1}$. Comparing with equation (27) for the peak intensity, it would take $\sim 10^7$ such detectors running for a year to detect the line distortion. The SPIRE instrument on *Herschel* will have a similar bolometer array, but with better beamsizes. The estimated sensitivity of $2.5\ \text{mJy}$ at 5σ in 1 hour for a $17.4\ \text{arcsec}$ FWHM beamsize (Griffin, Swinyard & Vigroux 2001) corresponds to $\lambda I_\lambda = 4.4 \times 10^{-8}\ \text{W m}^{-2}\text{sr}^{-1}$ per detector for the 1σ sensitivity in 1 second. So detection of the line would still require $\sim 10^6$ such detectors operating for a year.

These experiments are limited by thermal emission from the instrument itself, and so a significant advance would come from cooling the telescope. This is one of the main design goals of the proposed *SAFIR* (Leisawitz 2004) and *SPICA* (Nakagawa et al. 2004) missions. One can imagine improvements of a factor ~ 100 for far-IR observations with a cooled mirror. This would put us in the regime where arrays of $\sim 10^4$ detectors (of a size currently being manufactured for sub-mm instruments) could achieve the desired sensitivity.

One could imagine an experiment designed to have enough spectroscopic resolution to track the shape of the expected line distortion. The minimum requirement here is rather modest, with only $\lambda/\delta\lambda \sim 10$ in at least 3 bands. An important issue will be calibration among the different wavelengths, so that the non-thermal shape can be confidently measured. To overcome this, one might consider the use of direct spectroscopic techniques rather than filtered or frequency-sensitive bolometers.

Another way of quoting the required sensitivity is to say that any experiment which measures the recombination line distortion would have to measure the CIB spectrum with a precision of about 1 part in 10^5 , which is obviously a significant improvement over what can be currently achieved. A detection of the line distortion might therefore naturally come out of an extremely precise measurement of the CIB spectrum, which would also constrain other high frequency distortions to the CMB spectrum.

Some of the design issues involved in such an experiment are discussed by Fixsen & Mather (2002). They describe a future experiment for measuring deviations of the CMB spectrum from a perfect blackbody form, with an accuracy and precision of 1 part in 10^6 . This could provide upper limits on Bose-Einstein distortion μ and Compton distortion y parameters at the $\sim 10^{-7}$ level (the current upper limits for y and μ are 15×10^{-6} and 9×10^{-5} , respectively; Fixsen et al. 1996). The wavelength coverage they discuss is $2\text{--}120\ \text{cm}^{-1}$ (about $80\text{--}5,000\ \mu\text{m}$), which extends to much longer wavelengths than necessary for measuring the line

distortion. The beam-size would be large, similar to FIRAS, but the sensitivity achieved could easily be 100 times better. An experiment meant for detecting the line distortion would have to be another couple of orders of magnitude more sensitive still.

Turning to the second of the major challenges, it will be necessary to detect this line in the presence of the strong emission from our Galaxy. At $100\ \mu\text{m}$ the Galactic Plane can be as bright as $\sim 10^3\ \text{MJy sr}^{-1}$ which is about a billion times brighter than the signal we are looking for! Of course the brightness falls dramatically as one moves away from the Plane, but the only way to confidently avoid the Galactic foreground is to measure it and remove it. So any experiment designed to detect the line distortion will need to cover some significant part of the sky, so that it will be possible to extrapolate to the cosmological background signal. The spectrum of the foreground emission is likely to be smoother than that of the line distortion, and it may be possible to use this fact to effectively remove it. However, it seems reasonable to imagine that the most efficient separation of the signals will involve a mixture of spatial and spectral information, as is done for CMB data (see e.g. Patanchon et al. 2004).

In the language of spherical harmonics, the signal we are searching for is a monopole, with a dipole at the $\sim 10^{-3}$ level and smaller angular scale fluctuations of even lower amplitude. Hence we would expect to be extrapolating the Galactic foreground signals so that we can measure the overall DC level of the sky. This is made much more difficult by the presence of the CIB, which is also basically a monopole signal. Hence spatial information cannot be used to separate the line distortion from the CIB. The measurement of the line distortion is therefore made much more difficult by the unfortunate fact that the CIB is several orders of magnitude brighter – this is the third of the challenges in measuring the recombination lines.

The shape of the CIB spectrum is currently not very well characterised. It was detected using data from the DIRBE and FIRAS experiments on the *COBE* satellite. Estimates for the background (λI_λ) are: $9\ \text{nW m}^{-2}\text{sr}^{-1}$ at $60\ \mu\text{m}$ (Miville-Deschênes, Lagache & Puget 2002); $23\ \text{nW m}^{-2}\text{sr}^{-1}$ at $100\ \mu\text{m}$ (Lagache, Haffner & Reynolds 2000); $15\ \text{nW m}^{-2}\text{sr}^{-1}$ at $140\ \mu\text{m}$ (Lagache et al. 1999; Hauser et al. 1998); and $11\ \text{nW m}^{-2}\text{sr}^{-1}$ at $240\ \mu\text{m}$ (Lagache et al. 1999; Hauser et al. 1998). In each case the detections are only at the $3\text{--}5\sigma$ level, and the precise values vary between different prescriptions for data analysis (see also Schlegel, Finkbeiner & Davis 1998; Finkbeiner, Davis & Schlegel 2000; Hauser & Dwek 2001; Wright 2004). The short wavelength distortion of the CMB, interpreted as a measurement of the CIB (Puget et al. 1996) can be fit with a modified blackbody with temperature $18.5\ \text{K}$ and emissivity index 0.64 (although there is degeneracy between these parameters), which we plotted in Fig. 3.

The CIB is thus believed to peak somewhere around $100\ \mu\text{m}$, which is just about where we are expecting the recombination line distortion. The accuracy with which the CIB spectrum is known will have to improve by about 5 orders of magnitude before the distortion will be detectable. Fortunately the spectral shape is expected to be significantly narrower than that of the CIB – the line widths are similar to the $\delta z/z \sim 0.1$ for the last scattering surface thickness, as

opposed to $\delta\lambda/\lambda \sim 1$ for a modified blackbody shape (potentially even wider than this, given that the sources of the CIB come from a range of redshift $\Delta z \sim 1$).

One issue, however, is how smooth the CIB will be at the level of detail with which it will need to be probed. It may be that emission lines, absorption features, etc. could result in sufficiently narrow structure to obscure the recombination features. We are saved by 2 effects here: firstly the CIB averaged over a large solid angle patch is the sum of countless galaxies, and hence the individual spectral features will be smeared out; and secondly, the far-IR spectral energy distributions of known galaxies do *not* seem to contain strong features of the sort which might mimic the recombination distortion (see e.g. Lagache, Puget & Dole 2005). As we learn more about the detailed far-IR spectra of individual galaxies we will have a better idea of whether this places a fundamental limit on our ability to detect the recombination lines.

Overall it would appear that the line distortion should be detectable in principle, but will be quite challenging in practice.

5 CONCLUSIONS

We have studied the spectral distortion to the CMB due to the Ly α and 2s–1s two-photon transition of H and the corresponding lines of HeI and HeII. Together these lines give a quite non-trivial shape to the overall distortion. The strength and shape of the line distortions are very sensitive to the details of the recombination processes in the atoms. Although the amplitude of the spectral line is much smaller than the Cosmic Infrared Background, the raw precision required is within the grasp of current technology, and one can imagine designing an experiment to measure the non-trivial line shape which we have calculated. The basic detection of the existence of this spectral distortion would provide incontrovertible proof that the Universe was once a hot plasma and its amplitude would give direct constraints on physics at the recombination epoch.

6 ACKNOWLEDGMENTS

This research was supported by the Natural Sciences and Engineering Research Council of Canada. S.S. is supported by the Carnegie Institution of Washington. S.S. thanks John Bahcall for stimulating discussions. We thank Argyro Tasitomi for helping clarify Figure 1.

REFERENCES

Boschan P., Biltzinger P., 1998, *A&A*, 336, 1
 Burdyuzha V.V., Chekmezov A.N., 1994, *AZh*, 71, 341
 Burgin M.S., 2003, *AZh*, 80, 9, 771; English transl., 2003, *ARep*, 47, 709
 Chluba J., Sunyaev R. A., 2005, *A&A*, 446, 39
 Dell’Antonio I.P., Rybicki G.B., 1993, in *ASP Conf. Ser.* 51, *Observational Cosmology*, ed. G.Chincarini et al. (San Francisco:ASP), 548

Devlin M.J. et al., 2004, *Astronomical Structures and Mechanisms Technology*, ed. A. Joseph & D. Lemke, *Proc. SPIE*, Vol. 5498, p. 42
 Derevianko A., Johnson W.R., 1997, *Phys. Rev. A*, 56, 1288
 Drake G.W.F., Victor G.A., Dalgarno A., 1969, *Phys. Rev.*, 180, 25
 Drake G.W.F., 1986, *Phys. Rev. A*, 34, 2871
 Dubrovich V.K., 1975, *Pis'ma Astron. Zh.*, 1, 10, 3; English transl., 1975, *Sov. Astr. Lett.*, 1, 196
 Dubrovich V.K., Stolyarov V.A., 1995, *A&A*, 302, 635
 Dubrovich V.K., Stolyarov V.A., 1997, *Astrophys. Lett.*, 23, 565
 Dubrovich V.K., Grachev S.I., 2005, *Astronomy Letters*, 31, 359
 Fahr H.J., Loch R., 1991, *A&A*, 246, 1
 Finkbeiner D.P., Davis M., Schlegel D.J., 2000, *ApJ*, 544, 81
 Fixsen D.J., Cheng E.S., Gales J.M., Mather J.C., Shafer R.A., Wright E.L., 1996, *ApJ*, 473, 576
 Fixsen D.J., Dwek E., Mather J.C., Bennett C.L., Shafer R.A., 1998, *ApJ*, 508, 123
 Fixsen D.J., Mather J.C., 2002, *ApJ*, 581, 817
 Goldman S.P., 1989, *Phys. Rev. A*, 40, 1185
 Griffin M.J., Swinyard B.M., Vigroux L., 2001, *The Promise of the Herschel Space Observatory*, ed. G.L. Pilbratt, J. Cernicharo, A.M. Heras, T. Prusti & R. Harris, *ESA Special Publication* 460, 37
 Hauser M.G. et al., 1998, *ApJ*, 508, 25
 Hauser M.G., Dwek E., 2001, *Annu. Rev. Astron. Astrophys.*, 39, 249
 Hummer D.G., 1994, *MNRAS*, 268, 109
 Kholupenko E.E., Ivanchik A.V., Varshalovich D.A., 2005, www.ioffe.ru/astro/QC/CMBR/csmn.nc.pdf
 Lagache G., Abergel A., Boulanger F., Désert F.X., Puget J.-L., 1999, *A&A*, 344, 322
 Lagache G., Haffner L.M., Reynolds R.J., Tufte S.L., 2000, *A&A*, 354, 247
 Lagache G., Puget J.-L., Dole H., 2005, *ARA&A*, 43, 31
 Leisawitz D., 2004, *AdSpR*, 34, 631
 Leung P.K., Chan C.W., Chu M.C., 2004, *MNRAS*, 349, 2, 632
 Lipeles M., Novick R., Tolk N., 1965, *Phys. Rev. Lett.*, 15, 690
 Lyubarsky Y.E., Sunyaev R.A., 1983, *A&A*, 123, 171
 Martinis M., Stojic M., 2000, *FIZIKA A (Zagreb)*, 93, 115
 Mather J.C., Fixsen D.J., Shafer R.A., Mosier C., Wilkinson D.T., 1999, *ApJ*, 512, 511
 Miville-Deschênes M.-A., Lagache G., Puget J.-L., 2002 *A&A*, 393, 749
 Nakagawa T. et al, 2004, *AdSpR*, 34, 3, 645
 Padmanabhan T., 1993, *Structure Formation in the Universe*, Cambridge Univ. Press, Cambridge, UK
 Patanchon G., Cardoso J.-F., Delabrouille J., Vielva P., 2005, *MNRAS*, 364, 1185
 Peebles P.J.E. 1968, *ApJ*, 153, 1
 Peebles P.J.E., Seager S., Hu W., 2000, *ApJ*, 539, L1
 Pequignot D., Petitjean P., Boisson C., 1991, *A&A*, 251, 680
 Press W.H., Flannery B.P., Teukolsky S.A., Vetterling W.T., 1992, *Numerical Recipes in C: The Art of Scientific Computing*, Cambridge Univ. Press, Cambridge, UK
 Puget J.-L., Abergel A., Bernard J. -P., Boulanger F., Bur-

- ton W. B., Desert F. -X., Hartmann D., 1996, *A&A*, 308, L5
- Rubino-Martin J.A., Hernandez-Monteagudo C., Sunyaev R.A., 2005, *A&A*, 438, 461
- Santos J.P., Parente F., Indelicato P., 1998, *Eur. Phys. J.*, D3, 43
- Schlegel D.J., Finkbeiner D.P., Davis M., 1998, *ApJ*, 500, 525
- Scott D., Smoot G., 2004, *The Review of Particle Physics*, S. Eidelman et al., *Physics Letters B*.592,1
- Seager S., Sasselov D.D., Scott D., 1999, *ApJ*, 523, L1
- Seager S., Sasselov D.D., Scott D., 2000, *ApJS*, 128, 407
- Spergel D.N. et al., 2003, *ApJS*, 148, 175
- Spitzer L., Greenstein J.L.Jr., 1951, *ApJ*, 114, 407
- Switzer E.R., Hirata C.M., *Phys. Rev. D*, 72, 083002
- Tung J.H., Ye X.M., Salamo G.J., Chan F.T., 1984, *Phys. Rev. A*, 30, 1175
- Wright E.L., 2004, *New Astronomy Reviews*, 48, 465
- Zel'dovich Y.B., Kurt V.G., Sunyaev R.A., 1968, *Zh. Eksp. Teor. Fiz.*, 55, 278; English transl., 1969, *Soviet Phys. - JETP Lett.*, 28, 146

This paper has been typeset from a $\text{\TeX}/\text{\LaTeX}$ file prepared by the author.